A Four-Way Microstrip Filtering Power Divider With Frequency-Dependent Couplings

Feng-Jun Chen, Lin-Sheng Wu, *Senior Member, IEEE*, Liang-Feng Qiu, and Jun-Fa Mao, *Fellow, IEEE*

***Abstract*—A four-way microstrip power divider is designed with bandpass filtering response. The synthesized inline filter has a generalized Chebyshev response, where frequency-dependent couplings are utilized. All of the critical parameters, including the characteristic impedances and electrical lengths, can be determined by our derived closed-form formulas. By extending the inline filter, the configuration of four-way power divider is obtained. Then, three isolation resistors are properly selected according to the even-/odd-mode analysis. The proposed four-way filtering power divider has low in-band insertion loss and high frequency selectivity. It can provide the in-band return loss and isolation between outputs better than 16.7 and 17.5 dB, respectively.**

***Index Terms*—Filtering power divider, frequency-dependent coupling, general Chebyshev response, microstrip line, multifunctional passive component.**

I. Introduction

HIGH-PERFORMANCE miniaturized RF components with low cost and easy integration are desired in modern wireless communication systems. It is an effective method to achieve both small size and low insertion loss (IL) by integrating multiple functions into one component, which leads to a collaboratively designed multifunctional passive component. Since bandpass filter and power divider are two types of essential passives to select and divide/combine signals in various RF front-ends, respectively, power dividers with filtering responses have attracted much attention recently [1].

As Wilkinson and Gysel structures are two typical power-dividing topologies with high isolation between output ports and good impedance matching at all ports, most filtering power dividers are designed with these two configurations. The coupled resonator theory has been applied for the Wilkinson power dividers with narrow bandpass responses [2]–[5]. In [4], Wilkinson power dividers with Chebyshev and quasi-elliptic bandpass responses have been analyzed theoretically and realized with the net-type resonators. In order to improve the in-band isolation for higher order response, multiple isolation resistors should be applied in different stages, which is difficult for the implementation of cross-coupled topologies. Except for cross coupling, 0° feeding structure [2], mixed coupling [3], and tapped coupling [5] are adopted to get skirt frequency selectivity. Another design method is to use filtering structures as impedance transformers to replace the conventional $\lambda/4$ transmission lines in Wilkinson power dividers [6]–[8]. Unequal and dual-band Wilkinson power dividers integrated with bandpass responses are designed with proper filter structures in [6] and [7], respectively. Combinations of resistor and capacitor/inductor, instead of pure resistors, are used to get good isolation performance [7] or to reduce circuit size [8]. Their performance will be influenced by the accuracy and operating frequency of reactive elements. In addition, the ultra-wideband filtering power dividers have been proposed and designed with the even-/odd-mode method [9]–[11]. Recently, based on open-ended stubs and coupled lines, a four-way wideband filtering power divider is proposed and three resistors are used to achieve the isolation performance [12]. The circuit is very compact, but the reflection and isolation of output ports should be further improved. Based on the signal-interference technique and multistage structures, an eight-way single-band and a four-way quintuple-band power distribution networks are proposed in [13], but without considering the output isolation.

Bandpass filtering Gysel power dividers have also been proposed by using the coupled resonator theory [14], [15] and replacing $\lambda/4$ transmission lines with filtering structures [16]. However, it usually provides a second-order filtering response. More recently, the bandpass filtering characteristics of power dividers are extended to higher order by interconnecting the basic resonator-based building blocks, similar to a 180° hybrid coupler, with extra filter sections [17].

Till now, most reported filtering power dividers are focused on two-way applications. To the best of the authors' knowledge, only a few multiway components have been developed, including [12], [13], and [17].

High-frequency selectivity, low IL, and good in-band isolation are required for filtering power dividers. The realization of good reflection and isolation is usually a critical concern for filtering power dividers since the impedances of filters are significantly frequency-dependent around their passbands. Even for two-way cases, it is still difficult to achieve responses

Manuscript received January 28, 2015; revised June 15, 2015; accepted July 04, 2015. Date of publication August 04, 2015; date of current version October 02, 2015. This work was supported by the National Science Foundations of China under Grant 61370008 and Grant 61361166010.

F.-J. Chen was with the Key Laboratory of Ministry of Education of Design and Electromagnetic Compatibility of High-Speed Electronic Systems, Shanghai Jiao Tong University, Shanghai 200240, China. He is now with the Microsystem and Terahertz Research Center, China Academy of Engineering Physics, Chengdu 610200, China.

L.-S. Wu, L.-F. Qiu, and J.-F. Mao are with the Key Laboratory of Ministry of Education of Design and Electromagnetic Compatibility of High-Speed Electronic Systems, Shanghai Jiao Tong University, Shanghai 200240, China (e-mail: wallish@sjtu.edu.cn).

Color versions of one or more of the figures in this paper are available online at http://ieeexplore.ieee.org.

Digital Object Identifier 10.1109/TMTT.2015.2457426

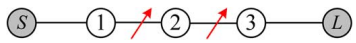

Fig. 1. Coupling scheme of a third-order inline bandpass filter with two frequency-dependent couplings.

as good as those of conventional power dividers. Complex isolation circuits should be applied to high-order filtering Wilkinson power dividers for good in-band isolation. For filtering Gysel power dividers and similar 180° filtering hybrid couplers, good isolation can be obtained by utilizing symmetric coupling schemes with many redundant resonators, leading to complicated topology and increased size [17]. Better frequency selectivity usually tends to need higher order response with more resonators, which will increase IL and circuit size. One economical way to improve frequency selectivity is to introduce transmission zeros (TZs) into lower order filters and filtering power dividers, which helps to reduce IL and size. Cross-coupled resonators are used in [2]–[4]. However, the cross-coupled filter topology is not suitable for the design of multiway filtering power dividers, which may require unrealizable cross couplings and isolation elements.

Other approaches to generate TZs include multimode resonator, nonresonating node, frequency-dependent (mixed) coupling, tapped structure, and so on. Among them, the frequency-dependent coupling is a promising technique, since it can provide TZs with inline topologies [18]–[20] and yield more TZs into cross-coupled topologies [21], [22]. The coupling matrix of frequency-dependent coupled generalized Chebyshev filter can be accurately synthesized by optimization technique and implemented in substrate integrated waveguide (SIW), microstrip, and waveguide [23]–[27]. A multiway power divider can be built up with fork structures directly [28] or realized by cascading several two-way power dividers with multiple isolation stages [29], [30]. It can be expected with good performance for an inline multiway filtering power divider based on frequency-dependent couplings and the cascading topology.

In this paper, a four-way bandpass filtering power divider is proposed. At first, an inline filter is synthesized with frequency-dependent couplings. Formulas are derived to determine the critical characteristic impedances and electrical lengths. Then, the filter is extended into a four-way power divider. According to the even-/odd-mode theory, the isolation resistors are well designed. A detailed procedure is concluded for the design of filtering power divider. The good performance of the proposed multifunctional component, such as high-frequency selectivity, good matching, and isolation, has been demonstrated by the simulated and measured results of the realized microstrip prototype.

II. Analysis and Design

A. Coupling Scheme and Matrix

The coupling scheme of a third-order inline bandpass filter is shown in Fig. 1, where the coupling between Resonators 1(2) and 2(3) is linearly frequency-dependent. The coupling matrix of the third-order filter can be synthesized by the zero-pole optimization method as [23], [24]

$$\begin{aligned}\mathbf{M}&=\mathbf{M}_0+\mathbf{M}_1\Omega\\&=\begin{bmatrix}0 & m_{S1}^0 & 0 & 0 & 0\\ m_{S1}^0 & m_{11}^0+m_{11}^1\Omega & m_{12}^0+m_{12}^1\Omega & 0 & 0\\ 0 & m_{12}^0+m_{12}^1\Omega & m_{22}^0+m_{22}^1\Omega & m_{23}^0+m_{23}^1\Omega & 0\\ 0 & 0 & m_{23}^0+m_{23}^1\Omega & m_{33}^0+m_{33}^1\Omega & m_{3L}^0\\ 0 & 0 & 0 & m_{3L}^0 & 0\end{bmatrix}.\end{aligned} \tag{1}$$

When the design specifications are given, the TZs can be assigned and the coupling matrix is then be synthesized. If the in-band return loss (RL) is set to 20 dB, and a pair of TZs are located at $-2.4j$ and $2.3j$ in the normalized frequency domain, the normalized coupling matrices are given by

$$\mathbf{M}_0=\begin{bmatrix}0 & 0.9442 & 0 & 0 & 0\\ 0.9442 & 0.8357 & 0.9922 & 0 & 0\\ 0 & 0.9922 & -0.0255 & -1.0023 & 0\\ 0 & 0 & -1.0023 & -0.8579 & 0.9333\\ 0 & 0 & 0 & 0.9333 & 0\end{bmatrix} \tag{2}$$

$$\mathbf{M}_1=\begin{bmatrix}0 & 0 & 0 & 0 & 0\\ 0 & 1 & 0.4134 & 0 & 0\\ 0 & 0.4134 & 1 & 0.4358 & 0\\ 0 & 0 & 0.4358 & 1 & 0\\ 0 & 0 & 0 & 0 & 0\end{bmatrix}. \tag{3}$$

According to the scaling procedure in [25], the normalized frequency-dependent coupling matrix can be renormalized for the design of resonators with different reactance/susceptance slope parameters, which is given by

$$\mathbf{M}\quad\Rightarrow\quad\begin{bmatrix}1 & & & & \\ & x_1 & & & \\ & & x_2 & & \\ & & & x_3 & \\ & & & & 1\end{bmatrix}\mathbf{M}\begin{bmatrix}1 & & & & \\ & x_1 & & & \\ & & x_2 & & \\ & & & x_3 & \\ & & & & 1\end{bmatrix} \tag{4}$$

where x_1, x_2, and x_3 are the scaling factors corresponding to different resonators. The S-parameters are kept unchanged during the scaling. The synthesis method in [25] is for the case of uniform slope parameters for all resonators. It is extended to the nonuniform case in this work to achieve more design freedom. For example, when the normalized slope parameters of three resonators are set to $k_1 = 1.6$, $k_2 = 2$, and $k_3 = 0.5$, the scaling factors of x_1, x_2, and x_3 can be solved from

$$\begin{cases}x_1^2-m_{12}^1x_1x_2=k_1\\ x_2^2-m_{12}^1x_1x_2-m_{23}^1x_2x_3=k_2\\ x_3^2-m_{23}^1x_2x_3=k_3\end{cases}. \tag{5}$$

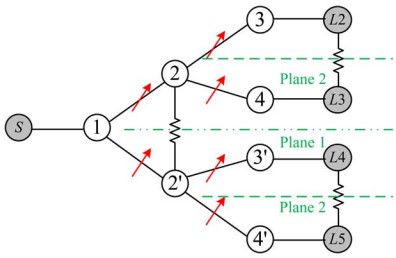

Fig. 2. Coupling scheme of a four-way filtering power divider based on the coupling scheme of the filter in Fig. 1.

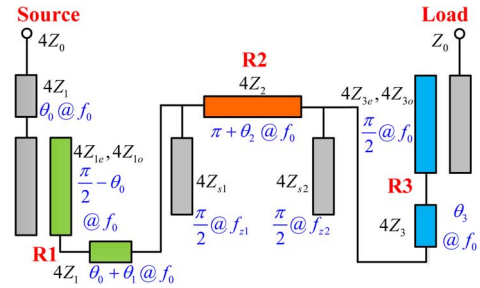

Fig. 3. Configuration of the third-order inline filter, where R1, R2 and R3 are the three resonators.

They are found as $x_1 = 1.8071$, $x_2 = 2.2297$ and $x_3 = 1.3438$. Then, the renormalized coupling matrices are calculated to be

$$\mathbf{M}_0 = \begin{bmatrix} 0 & 1.7063 & 0 & 0 & 0 \\ 1.7063 & 2.7292 & 3.9979 & 0 & 0 \\ 0 & 3.9979 & -0.1268 & -3.0031 & 0 \\ 0 & 0 & -3.0031 & -1.5491 & 1.2541 \\ 0 & 0 & 0 & 1.2541 & 0 \end{bmatrix} \tag{6}$$

$$\mathbf{M}_1 = \begin{bmatrix} 0 & 0 & 0 & 0 & 0 \\ 0 & 3.2657 & 1.6657 & 0 & 0 \\ 0 & 1.6657 & 4.9715 & 1.3057 & 0 \\ 0 & 0 & 1.3057 & 1.8057 & 0 \\ 0 & 0 & 0 & 0 & 0 \end{bmatrix}. \tag{7}$$

The scaling of the two coupling coefficients m_{12}^1 and m_{23}^1 can be approximated by

$$p \approx \frac{m_{12}^1\sqrt{k_1} + m_{23}^1\sqrt{k_3} + 2\sqrt{k_2}}{2 - \left(m_{12}^1\right)^2 - \left(m_{23}^1\right)^2} \tag{8}$$

$$m_{12}^1 \leftarrow \frac{1}{2}m_{12}^1 p\left[\sqrt{4k_1^2 + \left(m_{12}^1 p\right)^2} + m_{12}^1 p\right] \tag{9}$$

$$m_{23}^1 \leftarrow \frac{1}{2}m_{23}^1 p\left[\sqrt{4k_3^2 + \left(m_{23}^1 p\right)^2} + m_{23}^1 p\right]. \tag{10}$$

It can be seen that the values of scaled m_{12}^1 and m_{23}^1 will increases with k_1, k_2, and k_3.

Based on the coupling scheme and matrices of the third-order inline filter, a four-way filtering power divider can be constructed. It has two two-way power dividing stages and three isolation resistors, as shown in Fig. 2. The power divider has two sets of symmetric planes, i.e., Plane 1 and Plane 2. When all of the symmetric planes are assumed as magnetic walls, the filter can be regarded as the equivalent even–even quarter circuit of the power divider. Then, the input matching and transmission performances are properly designed. By further carefully considering the other equivalent quarter circuits for even–odd, odd–even, and odd–odd cases, the output matching and isolation performances can also be achieved.

B. Synthesis of Inline Bandpass Filter

In order to implement the equivalent even–even filter of the filtering power divider, the configuration shown in Fig. 3 is proposed. It consists of a half-wavelength resonator and two quarter-wavelength resonators. For the transformation from the four-way power divider, the reference impedances of the two filter ports are set to $4Z_0 = 200\,\Omega$ and $Z_0 = 50\,\Omega$. The factor 4 of the characteristic impedances is for simple analysis of the four-way power divider. The incremental electrical lengths θ_1, θ_2, and θ_3 finely control the frequency shifts of resonators from the central frequency. The positive frequency-dependent couplings between adjacent resonators are realized by open-ended stubs, which have approximately linear frequency variation within the frequency range of interest. The frequency-invariant external couplings are realized by open-ended coupled lines.

Frequency and impedance transformations should be adopted for the bandpass filter designed with the coupling matrices of (6) and (7). In our design, the central frequency is $f_0 = 2$ GHz and the fractional bandwidth is FBW $= 6\%$. When the following condition is satisfied:

$$m_{12}^1 \frac{1}{\mathrm{FBW}}\left(\frac{f_{z1}}{f_0} - \frac{f_0}{f_{z1}}\right) + m_{12}^0 = 0 \tag{11}$$

the coupling between Resonators 1 and 2 will be dismissed. Thus, the reference frequency of the first open-ended stub is obtained to be $f_{z1} = 1.86$ GHz, and its electrical length is $\pi/2$. Similarly, when

$$m_{23}^1 \frac{1}{\mathrm{FBW}}\left(\frac{f_{z2}}{f_0} - \frac{f_0}{f_{z2}}\right) + m_{23}^0 = 0 \tag{12}$$

is satisfied, we have $f_{z2} = 2.14$ GHz also with the electrical length of $\pi/2$. In the inline topology, the two reference frequencies of stubs are equal to the desired TZs of the filter, i.e. $-2.4j$ and $2.3j$.

The input impedance of the two stubs are

$$Z_{\mathrm{ins},p} = -j4Z_{s,p}\cot\frac{\pi f}{2f_{z,p}} \tag{13}$$

where $p = 1$ and 2. They can be regarded as K-inverters with residual series impedances, as shown in Fig. 4. The first-order Taylor approximation of $Z_{\mathrm{ins},p}$ around the central frequency is

$$\begin{aligned} Z_{\mathrm{ins},p} &\approx Z_{\mathrm{ins},p}^0 + \Omega Z_{\mathrm{ins},p}^1 \\ &\approx -j4Z_{s,p}\cot\frac{\pi f_0}{2f_{z,p}} + j\Omega FBW\frac{\pi f_0}{f_{z,p}}Z_{s,p}\csc^2\frac{\pi f_0}{2f_{z,p}} \end{aligned} \tag{14}$$

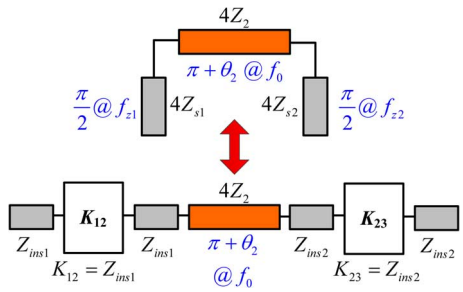

Fig. 4. Equivalent circuit of the open-ended stubs and Resonator 2.

where the normalized radian frequency is approximated by

$$\Omega=\frac{1}{\mathrm{FBW}}\left(\frac{f}{f_0}-\frac{f_0}{f}\right)\approx\frac{2\left(f-f_0\right)}{f_0\mathrm{FBW}}. \tag{15}$$

Then, the input impedance of Resonator 2 looked from the K_{12}-inverter is calculated by

$$Z_{\mathrm{inr2}}=Z_{\mathrm{ins1}}+4Z_2\frac{Z_{ins2}+j4Z_2\tan\left[\left(\pi+\theta_2\right)\frac{f}{f_0}\right]}{4Z_2+jZ_{\mathrm{ins2}}\tan\left[\left(\pi+\theta_2\right)\frac{f}{f_0}\right]} \tag{16}$$

The first-order approximation is given by

$$Z_{\mathrm{inr2}}\approx Z^0_{\mathrm{inr2}}+\Omega Z^1_{\mathrm{inr2}} \tag{17}$$
$$Z^0_{\mathrm{inr2}}\approx Z^0_{\mathrm{ins1}}+Z^0_{\mathrm{ins2}}+j4Z_2\tan\theta_2 \tag{18}$$
$$Z^1_{\mathrm{inr2}}\approx Z^1_{\mathrm{ins1}}+Z^1_{\mathrm{ins2}}+jFBW(\pi+\theta_2)2Z_2\sec^2\theta_2. \tag{19}$$

Comparing (14)–(19) with (1), (6), and (7), one can conclude that

$$\begin{aligned}-\frac{4Z_{s1}\cot\frac{\pi f_0}{2f_{z1}}}{m^0_{12}}&=-\frac{4Z_{s2}\cot\frac{\pi f_0}{2f_{z2}}}{m^0_{23}}\\&=\frac{4Z_2\tan\theta_2}{m^0_{22}-m^0_{12}-m^0_{23}}\\&=\frac{FBW\frac{\pi f_0}{f_{z1}}Z_{s1}\csc^2\frac{\pi f_0}{2f_{z1}}}{m^1_{12}}\\&=\frac{FBW\frac{\pi f_0}{f_{z2}}Z_{s2}\csc^2\frac{\pi f_0}{2f_{z2}}}{m^1_{23}}\\&=\frac{FBW\left(\pi+\theta_2\right)2Z_2\sec^2\theta_2}{k_2}=x_0.\end{aligned} \tag{20}$$

If the common ratio is set to the reference reactance parameter $x_0=\pi Z_0\mathrm{FBW}$, which can simplify the calculation of characteristic impedances, the related characteristic impedances and electrical length can be determined by

$$\begin{aligned}Z_{s1}&=\frac{f_{z1}x_0}{\pi f_0\mathrm{FBW}}\sin^2\left(\frac{\pi}{2}\frac{f_0}{f_{z1}}\right)m^1_{12}\\&=\frac{f_{z1}}{f_0}Z_0\sin^2\left(\frac{\pi}{2}\frac{f_0}{f_{z1}}\right)m^1_{12}\end{aligned} \tag{21}$$

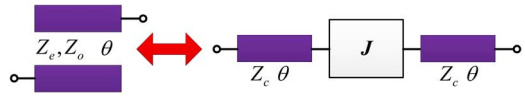

Fig. 5. Equivalent circuits of the coupled line for external coupling.

$$\begin{aligned}Z_{s2}&=\frac{f_{z2}x_0}{\pi f_0\mathrm{FBW}}\sin^2\left(\frac{\pi}{2}\frac{f_0}{f_{z2}}\right)m^1_{23}\\&=\frac{f_{z2}}{f_0}Z_0\sin^2\left(\frac{\pi}{2}\frac{f_0}{f_{z2}}\right)m^1_{23}\end{aligned} \tag{22}$$

$$Z_2=\frac{x_0\cos^2\theta_2}{2\left(\pi+\theta_2\right)\mathrm{FBW}}k_2\approx\frac{k_2}{2}Z_0 \tag{23}$$

$$\theta_2\approx\arctan\left[\frac{\pi\mathrm{FBW}}{2k_2}\left(m^0_{22}-m^0_{12}-m^0_{23}\right)\right] \tag{24}$$

where the approximation of Z_2 is based on the assumption of θ_2 usually with a small value. Then, the reactance slope parameter of Resonator 2 is derived as

$$x_{r2}=\frac{f_0}{2}\left.\frac{\partial\mathrm{Im}(Z_{\mathrm{inr2}})}{\partial f}\right|_{f=f_0}=\frac{\mathrm{Im}\left(Z^1_{\mathrm{inr2}}\right)}{\mathrm{FBW}}\approx\frac{x_0m^1_{22}}{\mathrm{FBW}}. \tag{25}$$

It is found that the calculation of the reference frequencies f_{z1} and f_{z2} of stubs is the same as [25], but the equations of (21)-(24) for characteristic impedances and electrical length are different from those in [25]. The characteristic impedances in our design are $Z_{s1}=76.4\,\Omega$, $Z_{s2}=69.2\,\Omega$, and $Z_2=50\,\Omega$. The incremental electrical length of Resonator 2 is $\theta_2=-3.03^\circ$.

Two coupled lines are used for external couplings, which can be analyzed with the equivalent circuit in Fig. 5. By equating the related transmission matrices, we have

$$\frac{\sqrt{(Z_e-Z_o)^2-(Z_e+Z_o)^2\cos^2\theta}}{2\sin\theta}=\sqrt{\frac{JZ_c^2\sin^2\theta-\frac{1}{J}\cos^2\theta}{\frac{1}{JZ_c^2}\sin^2\theta-J\cos^2\theta}} \tag{26}$$

$$\frac{Z_e+Z_o}{Z_e-Z_o}=\left(JZ_c+\frac{1}{JZ_c}\right)\sin\theta \tag{27}$$

where the difference between the even- and odd-mode electrical lengths is ignored. For the external coupling between Source and Resonator 1, the electrical length of the coupled line is $\theta=\pi/2-\theta_0$ and the characteristic impedances are $Z_c=4Z_1$, $Z_e=4Z_{1e}$, and $Z_o=4Z_{1o}$. For the external coupling between Resonator 3 and Load, the parameters are $\theta=\pi/2$, $Z_c=4Z_3$, $Z_e=4Z_{3e}$, and $Z_o=4Z_{3o}$. When the values of θ and Z_c are given, the even-/odd-mode impedances of coupled line are obtained by

$$\begin{aligned}Z_e=&\frac{\left(JZ_c+\frac{1}{JZ_c}\right)\sin^2\theta+\sin\theta}{\sqrt{1-\left(JZ_c+\frac{1}{JZ_c}\right)^2\sin^2\theta\cos^2\theta}}\\&\times\sqrt{\frac{JZ_c^2\sin^2\theta-\frac{1}{J}\cos^2\theta}{\frac{1}{JZ_c^2}\sin^2\theta-J\cos^2\theta}}\end{aligned} \tag{28}$$

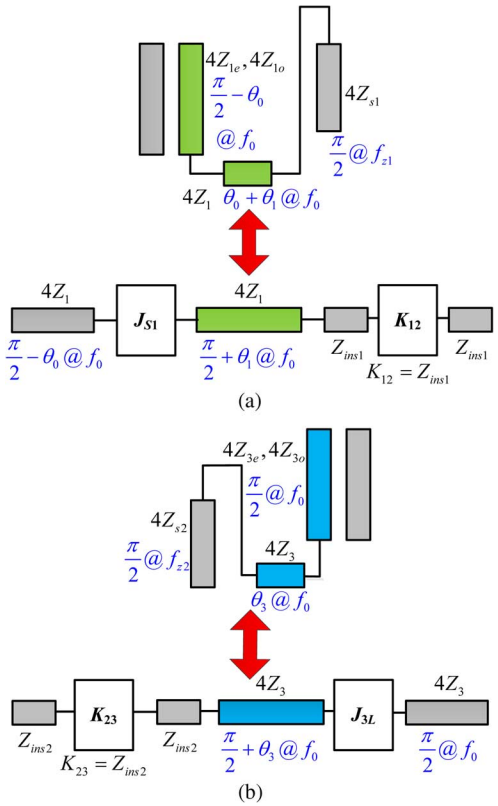

Fig. 6. Equivalent circuit models of (a) Resonator 1 and (b) Resonator 3.

$$Z_o=\frac{\left(JZ_c+\frac{1}{JZ_c}\right)\sin^2\theta-\sin\theta}{\sqrt{1-\left(JZ_c+\frac{1}{JZ_c}\right)^2\sin^2\theta\cos^2\theta}}\times\sqrt{\frac{JZ_c^2\sin^2\theta-\frac{1}{J}\cos^2\theta}{\frac{1}{JZ_c^2}\sin^2\theta-J\cos^2\theta}}. \tag{29}$$

The equivalent circuit models of Resonators 1 and 3 are shown in Fig. 6. According to Fig. 6(a), the input impedance of Resonator 1 looked from the first stub can be written as

$$Z_{\text{inr1}}=Z_{ins1}-j4Z_1\cot\left[\left(\frac{\pi}{2}+\theta_1\right)\frac{f}{f_0}\right]. \tag{30}$$

It is first-order approximated by

$$Z_{inr1}\approx Z^0_{\text{inr1}}+\Omega Z^1_{\text{inr1}} \tag{31}$$
$$Z^0_{\text{inr1}}=Z^0_{\text{ins1}}+j4Z_1\tan\theta_1 \tag{32}$$
$$Z^1_{\text{inr1}}=Z^1_{\text{ins1}}+j\text{FBW}\left(\frac{\pi}{2}+\theta_1\right)2Z_1\sec^2\theta_1. \tag{33}$$

Similar to (20), (23), and (24), we have

$$Z_1=\frac{x_0\cos^2\theta_1}{2\left(\frac{\pi}{2}+\theta_1\right)FBW}k_1\approx k_1Z_0 \tag{34}$$
$$\theta_1\approx\arctan\left[\frac{\pi FBW}{4k_1}\left(m^0_{11}-m^0_{12}\right)\right]. \tag{35}$$

According to Fig. 6(b), it is derived that

$$Z_3=\frac{x_0\cos^2\theta_3}{2\left(\frac{\pi}{2}+\theta_3\right)FBW}k_3\approx k_3Z_0 \tag{36}$$
$$\theta_3\approx\arctan\left[\frac{\pi FBW}{4k_3}\left(m^0_{33}-m^0_{23}\right)\right]. \tag{37}$$

Therefore, the parameters of Resonators 1 and 3 are obtained as $Z_1=80\,\Omega$, $\theta_1=-2.14°$, $Z_3=25\,\Omega$ and $\theta_3=7.80°$. Further, the related reactance slope parameters are also approximated by

$$x_{ri}\approx\frac{x_0m^1_{ii}}{\text{FBW}} \tag{38}$$

where $i=1$, 2, and 3.

The input admittance of Resonator 1 looked from the J_{S1}-inverter is

$$Y_{\text{inr1}}=\frac{1}{4Z_1}\frac{4Z_1+jZ_{\text{ins1}}\tan\left[\left(\frac{\pi}{2}+\theta_1\right)\frac{f}{f_0}\right]}{Z_{\text{ins1}}+j4Z_1\tan\left[\left(\frac{\pi}{2}+\theta_1\right)\frac{f}{f_0}\right]}$$
$$\approx Y^0_{\text{inr1}}+\Omega Y^1_{\text{inr1}} \tag{39}$$
$$Y^0_{\text{inr1}}\approx\frac{Z^0_{\text{ins1}}}{16Z_1^2}+j\frac{4Z_1\tan\theta_1}{16Z_1^2} \tag{40}$$
$$Y^1_{\text{inr1}}\approx\frac{Z^1_{ins1}}{16Z_1^2}+j\frac{\text{FBW}\left(\frac{\pi}{2}+\theta_1\right)2Z_1\sec^2\theta_1}{16Z_1^2}. \tag{41}$$

Comparing (37)–(39) with (30)–(32), it is found that

$$Y_{\text{inr1}}\approx\frac{Z_{\text{inr1}}}{16Z_1^2} \tag{42}$$

which means the coupling matrices can be used as both impedance and admittance matrices. Then, the susceptance slope parameter of Resonator 1 can be obtained from (42) and (38) as

$$b_{r1}\approx\frac{x_0m^1_{11}}{16Z_1^2\text{FBW}}. \tag{43}$$

As shown in Fig. 7(a), the input admittance of Source combined with the J_{S1}-inverter, looked from Resonator 1, is

$$Y_{eS}=\frac{4J^2_{S1}Z_1^2}{Z_0} \tag{44}$$

The external Q-factor of Source is given by

$$Q_{eS}=\frac{b_1}{Y_{eS}}=\frac{Z_0x_0m^1_{11}}{64J^2_{S1}Z_1^4\text{FBW}} \tag{45}$$

It should be equal to the value calculated from the coupling matrix, i.e.,

$$Q_{eS}=\frac{m^1_{11}}{\left(m^0_{S1}\right)^2\text{FBW}}. \tag{46}$$

Therefore, it can be derived as

$$J_{S1}=\frac{m^0_{S1}}{8Z_1^2}\sqrt{Z_0x_0}=\frac{m^0_{S1}}{8k_1^2Z_0}\sqrt{\pi\text{FBW}}. \tag{47}$$

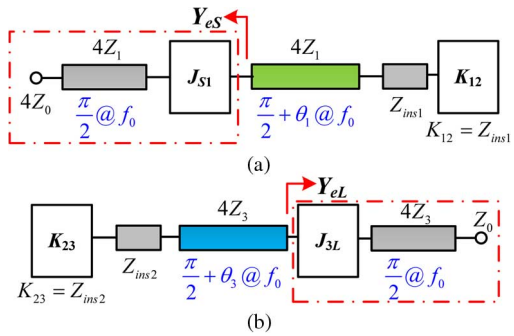

Fig. 7. Equivalent circuits for the external coupling of (a) Source and (b) Load.

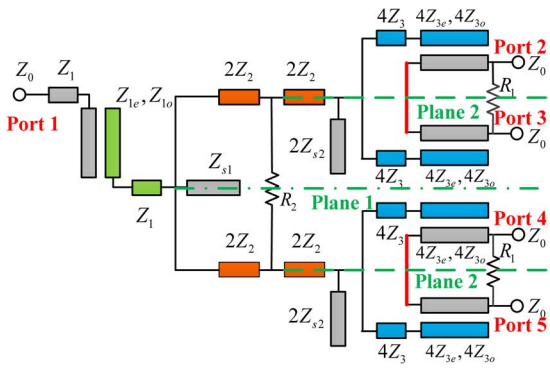

Fig. 8. Configuration of the four-way filtering power divider based on frequency-dependent couplings.

Similarly, the inverter value of Load can be deduced with the equivalent circuit in Fig. 7(b), which is

$$J_{3L}=\frac{m_{3L}^0}{16k_3^2Z_0}\sqrt{\pi \mathrm{FBW}}. \tag{48}$$

For the coupled line at Source, the electrical length of the short transmission line is assigned to $\theta_0=23°$. Then, the even- and odd-mode characteristic impedances are calculated to be $4Z_{1e}=421.6\,\Omega$ and $4Z_{1o}=259.2\,\Omega$, based on (28), (29), (34), and (47). For the coupled line at Load, the even- and odd-mode characteristic impedances are given by $4Z_{3e}=134.6\,\Omega$ and $4Z_{3o}=80.2\,\Omega$, with (28), (29), (36), and (48). In this way, all of the parameters in Fig. 3 have been synthesized for the bandpass filter based on frequency-dependent couplings.

C. Four-Way Power Divider with Filtering Response

As shown in Fig. 8, a four-way resonator-coupled power divider is realized according to the coupling scheme in Fig. 2 and the configuration of the filter in Fig. 3. In comparison with the proposed filter, the characteristic impedances of the power divider are divided by the factors of 4, 2, and 1 for different stages, while all of the electrical lengths are kept unchanged. For good isolation, two resistors of R_1 are located between Ports 2(4) and 3(5) and a resistor of R_2 is loaded between Resonators 2 and $2'$. The open ends of four output ports are connected in pairs (marked with red lines in Fig. 8), which does not affect the filtering response of the equivalent even-even quarter circuit.

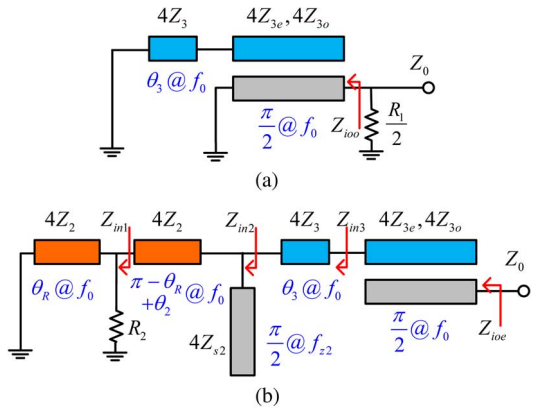

Fig. 9. Equivalent circuits: (a) the quarter circuit for both the even–odd and odd–odd cases and (b) the quarter circuit for the odd–even case.

Due to the topological symmetry of the structure, the S-parameters of the power divider can be analyzed with the even-/odd-mode method as [29]

$$S_{11}=S_{11ee} \tag{49}$$

$$S_{21}=S_{31}=S_{41}=S_{51}=\frac{S_{21ee}}{2} \tag{50}$$

$$S_{22}=\left(\frac{S_{22ee}}{4}+\frac{S_{22eo}}{4}\right)+\left(\frac{S_{22oe}}{4}+\frac{S_{22oo}}{4}\right) \tag{51}$$

$$S_{32}=\left(\frac{S_{22ee}}{4}-\frac{S_{22eo}}{4}\right)+\left(\frac{S_{22oe}}{4}-\frac{S_{22oo}}{4}\right) \tag{52}$$

$$S_{42}=S_{52}=\left(\frac{S_{22ee}}{4}\pm\frac{S_{22eo}}{4}\right)-\left(\frac{S_{22oe}}{4}\pm\frac{S_{22oo}}{4}\right) \tag{53}$$

where the first and second subscripts correspond to the symmetric Planes 1 and 2, respectively. The even–even quarter circuit is just the filter configuration analyzed in Section II.B, and S_{22ee} is just the reflection coefficient at Port 2 of the filter prototype. The equivalent quarter circuits of other cases are shown in Fig. 9. Note that, when Plane 2 is set to an electrical wall, the quarter circuits for the even–odd and odd–odd cases are the same as each other, as shown in Fig. 9(a). Therefore, it always satisfies that $S_{22eo}=S_{22oo}$, leading to $S_{42}=S_{52}=(S_{22ee}-S_{22oe})/4$. In order to achieve good matching and isolation for output ports, one can conclude from (51)–(53) that both S_{22oe} and S_{22oo} should be sufficiently small.

When Plane 2 is set an electrical wall, the equivalent quarter circuit is shown in Fig. 9(a). The input impedance excluding the resistor is given by

$$Z_{ioo}=Z_{22}-\frac{Z_{21}^2}{Z_{11}+j4Z_3\tan\left(\frac{\theta_3 f}{f_0}\right)} \tag{54}$$

where

$$Z_{11}=-j\frac{8Z_{3e}Z_{3o}}{Z_{3e}+Z_{3o}}\cot\frac{\pi f}{2f_0} \tag{55}$$

$$Z_{21}=0 \tag{56}$$

$$Z_{22}=j2\left(Z_{3e}+Z_{3o}\right)\tan\frac{\pi f}{2f_0}. \tag{57}$$

The input impedance Z_{ioo} is infinite at the central frequency f_0. Then, for $S_{22eo} = S_{22oo} = 0$, it is obtained that $R_1 = 2Z_0 = 100$ ohm. With the above assignment of R_1, $S_{22eo} = S_{22oo}$ are smaller than -35 dB in the whole passband. Then, the output reflection and isolation are mainly determined by S_{22ee} and S_{22eo}, which should be both sufficiently small.

The input impedance Z_{ioe} of the odd–even quarter circuit in Fig. 9(b) can be calculated at the central frequency f_0 by

$$Z_{\text{in1}} = j4Z_2 \tan\left[\frac{\theta_R f}{f_0}\right] // R_2 \tag{58}$$

$$Z_{\text{in2}} = 4Z_2 \frac{Z_{\text{in1}} + j4Z_2 \tan\left[(\theta'_R + \theta_2)\frac{f}{f_0}\right]}{4Z_2 + jZ_{\text{in1}} \tan\left[(\theta'_R + \theta_2)\frac{f}{f_0}\right]} // \left[-j4Z_{s2} \cot\left(\frac{\pi}{2}\frac{f}{f_{z2}}\right)\right] \tag{59}$$

$$Z_{\text{in3}} = 4Z_3 \frac{Z_{in2} + j4Z_3 \tan\left(\frac{\theta_3 f}{f_0}\right)}{4Z_3 + jZ_{\text{in2}} \tan\left(\frac{\theta_3 f}{f_0}\right)} \tag{60}$$

$$Z_{ioe} = -j2\left(Z_{3e} + Z_{3o}\right)\cot\theta + \frac{4\left(Z_{3e} - Z_{3o}\right)^2 \csc^2\theta}{Z_{\text{in3}} - j2\left(Z_{3e} + Z_{3o}\right)\cot\theta} \tag{61}$$

where θ_R is the electrical length of the transmission line from the first open stub to the location of resistor R_2 at the central frequency, $\theta'_R = \pi - \theta_R$ and $\theta = \pi f/(2f_0)$. The refection coefficient of odd–even case is

$$S_{22oe} = \frac{Z_{ioe} - Z_0}{Z_{ioe} + Z_0}. \tag{62}$$

The response of S_{22oe} can be controlled by the location θ_R and resistance R_2. Fig. 10(a) shows the synthesized results of S_{22}, S_{32}, and S_{42} with different θ_R of 45°, 90°, and 135°. For each electrical length, the resistance R_2 is optimized to achieve the best responses. The calculated S_{22oe} with (58)–(62) is shown in Fig. 11. It is seen that S_{22oe} can be small within a narrow band by properly selecting θ_R and R_2. The case of 135° shows better in-band performance than the others. The results with a small variation of θ_R are shown in Fig. 10(b), where the responses are not much changed. Thus, the in-band RL and output isolation are not very sensitive to the loading of R_2 when θ_R is around 135°. In this way, the location and resistance of R_2 are determined. Since the response of S_{22oe} is determined analytically, the optimization will be very efficient. Here, R_2 is optimized to about 680 Ω.

In this way, all the critical parameters in Figs. 3 and 9 are determined. The synthesized results are plotted in Fig. 12. It is seen that a good bandpass filtering response is achieved with good transmission and reflection of the input port. The RL at output ports and the isolation between Ports 2 and 3 are about 28.4 dB at the central frequency, where the isolation between Ports 2 and 4 is about 29.7 dB. Within the whole passband, the synthesized RL and output isolation are better than 19 and 20 dB, respectively.

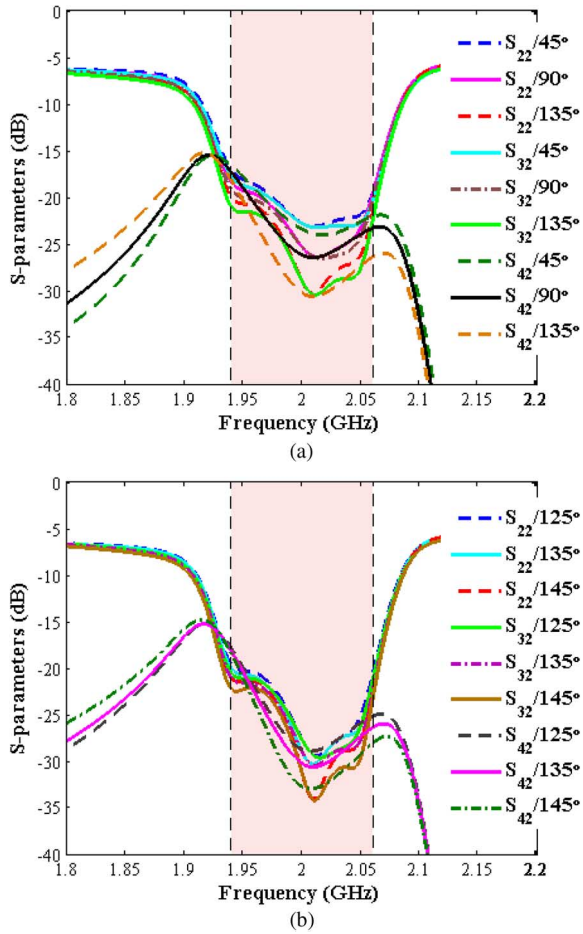

Fig. 10. Synthesized results of S_{22}, S_{32}, and S_{42} with different θ_R: (a) within a large variation from 45° to 135° and (b) within a small variation around 135°.

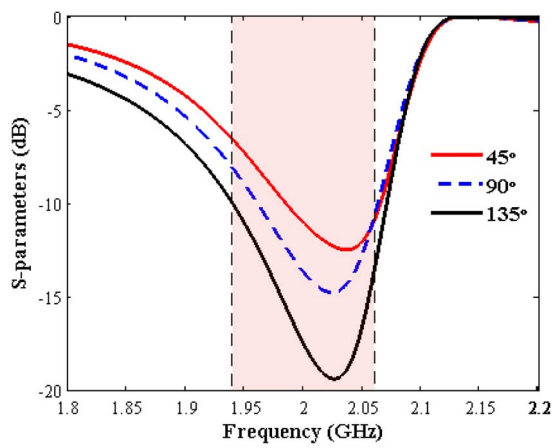

Fig. 11. Calculated responses of S_{22oe} with different values of θ_R.

D. Design Procedure

Therefore, the proposed bandpass filtering power divider can be developed according to the following steps.

Step 1) Synthesize the normalized coupling matrices (2) and (3) with the preset coupling scheme, for the design specifications, including the central frequency f_0, the fractional bandwidth FBW, the in-band RL,

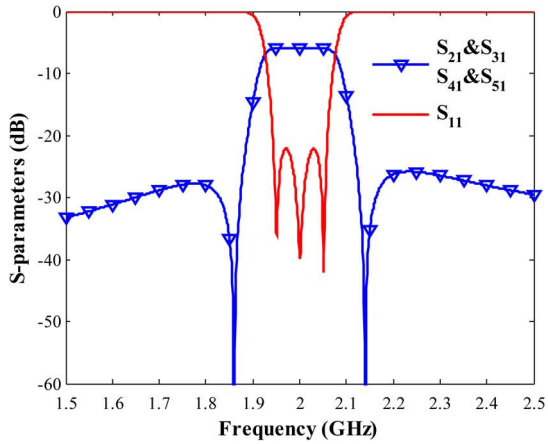

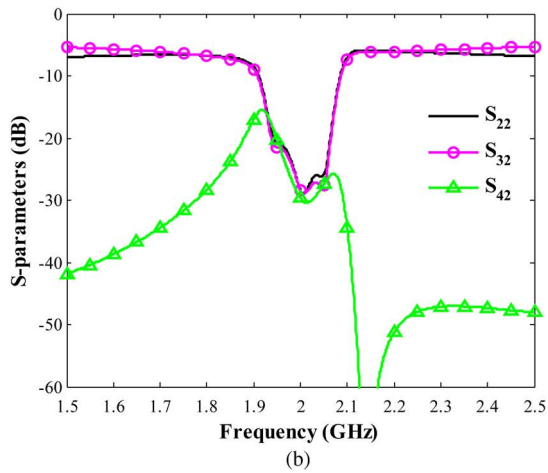

Fig. 12. Synthesized results of the filtering power divider: (a) the insertion loss and return loss at input port; and (b) the return loss and isolation of outputs.

and the locations of TZs. The optimization technique is based on the eigenvalues of linear matrix pencils.

Step 2) Considering the realizable range of characteristic impedance of transmission line, set the normalized slope parameters of resonators, i.e., k_1, k_2, and k_3. Solve the scaling factors of x_1, x_2, and x_3 with (5) and renormalize the coupling matrices as (6) and (7).

Step 3) Set the reference reactance slope parameter to $x_0 = \pi Z_0 \mathrm{FBW}$, and then calculate the characteristic impedances Z_1, Z_2, Z_3, Z_{s1}, and Z_{s2} of transmission-line resonators and open-ended stubs with (21)–(23), (34), and (36). All of the characteristic impedances will increase with the normalized slope parameters. According to the topology of our filtering power divider, the characteristic impedances $4Z_3$ and $2Z_{s2}$ of Resonator 3 and the second stub are usually with the relatively high values, which are mainly determined by k_3. Thus, a small k_3 is preferred. The incremental electrical lengths θ_1, θ_2 and θ_3 are obtained with (24), (35), and (37). The reference frequencies of the stubs are determined by (11) and (12).

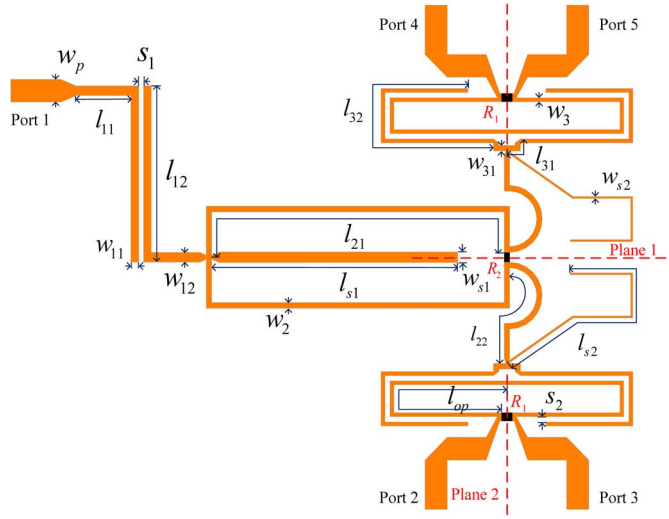

Fig. 13. Layout of the proposed four-way filtering power divider prototype.

Step 4) Calculate the inverter values J_{S1} and J_{3L} for the input and output external couplings with (47) and (48), respectively. Obtain the even- and odd-mode characteristic impedances of the input and output coupled lines with (28) and (29). For the input coupled line, a suitable value of θ_0 is set in advance.

Step 5) Construct a four-way filtering power divider based on the bandpass filter with two power-dividing stages. The isolation resistor R_1 is selected to be $2Z_0 = 100\ \Omega$. The location θ_R of the resistor R_2 are explored numerically within a large range, and the resistance R_2 is optimized to achieve small magnitude of S_{22oe} within the passband for each value of θ_R. By properly selecting θ_R and R_2, the best output reflection and isolation can be found.

Step 6) Develop the layout and physical dimensions for the filtering power divider. Full-wave simulation and optimization may be required to achieve good performances of transmission, input and output matching, isolation and magnitude/phase balances between the output ports.

III. Results and Discussion

As shown in Fig. 13, a filtering power divider prototype is designed and fabricated on a Taconic RF-35A2 substrate, with the relative dielectric constant of $\varepsilon_r = 3.5$, the thickness of $h = 40$ mil and the dielectric loss tangent of $\tan\delta = 0.0015$. After the full-wave simulations and optimization by using ANSYS HFSS, the dimensions of the prototype are obtained, as summarized in Table I. The overall size is 66.05×48.97 mm^2. The isolation resistors are $R_1 = 100\ \Omega$ and $R_2 = 680\ \Omega$.

The simulated and measured results are shown in Fig. 14. In Fig. 14(a), the simulated and measured central frequency is 2.0 and 1.992 GHz, respectively. The measured minimum IL is 6 + 1.1 dB while the simulated is 6+0.83 dB. The small difference is introduced by the SMA connectors used in measurements. The RL of input port is larger than 19 dB in the passband from 1.94 to 2.06 GHz for both simulations and measurements.

TABLE I
GEOMETRIC PARAMETERS OF THE FILTERING POWER DIVIDER (UNIT: MM)

Symbol	Quantity	Symbol	Quantity
w_p	2.21	s_1	0.46
l_{11}	5.47	w_{31}	0.56
l_{12}	17.11	w_3	0.39
w_{11}	0.95	l_{31}	1.99
w_{12}	0.79	l_{32}	24.37
w_{s1}	1.05	w_{s2}	0.20
l_{s1}	24.51	l_{s2}	24.23
w_2	0.56	s_2	0.51
l_{21}	38.58	l_{op}	25.46
l_{22}	14.09		

The measured RLs of output ports are better than 16.7 dB in passband, as shown in Fig. 14(b). From Fig. 14(c), it is seen that the measured isolation between the output ports is greater than 17.5 dB over the passband. The deviation from synthesized response is mainly resulted from the asynchronous tuning of Resonators 1 and 3 the filtering power divider while the slight frequency shift of measured results from the simulated ones is caused by the tolerance of substrate parameter and fabrication. The performance degradations are mainly due to the fabrication tolerance, especially sensitive to physical dimensions of the input and output coupled lines.

The measured imbalances between output ports are shown in Fig. 14(d). The magnitude imbalance is from -0.02 to 0.44 dB and the phase imbalance is from 0.84° to 5° within the passband. The magnitude imbalance of S_{41}/S_{21} is greater than that of S_{31}/S_{21}, which is found in both the measured and full-wave simulated results, but not indicated by the synthesized one. In our synthesis, the circuit is set with ideal symmetry property, which leads to perfect balance performance. In our layout, the coupled line of external coupling between Source and Resonator 1 is not arranged symmetric to the middle plane of the whole circuit. Ports 4 and 5 are closer to Port 1 than Ports 2 and 3, as shown in Fig. 13. Therefore, parasitic couplings may exist to introduce the magnitude imbalance of 0.3 to 0.4 dB.

The size and performance of our proposed inline filtering power divider, based on frequency-dependent couplings, are compared with those of the previously reported four-way counterparts in Table II, where λ_g means the guided wavelength of 50-Ω microstrip lines at corresponding central frequencies on substrates. The filtering power divider in [12] is developed for wideband application and occupies the smallest area, but the in-band RL and output isolation are only better than 10 and 12 dB, respectively. Both the four-way power distribution networks in [13] and [17] are with much larger circuit sizes than the proposed component. Although the layout might be further miniaturized, the isolation between outputs is not considered when designing the quintuple-band four-way network in [13]. In [17], the paths from Port 1 to Ports 3 to 6 of the eight-port SIW power divider show a four-way fifth-order filtering power dividing performance. In this case, Ports 2, 7, and 8 and six redundant SIW cavities, as shown in [17, Fig. 12], are utilized to construct several basic building blocks for good isolation. Therefore, the circuit size of such multiport power distribution networks will consequently be larger than the Wilkinson counterparts in [12] and this work. Due to the utilization of basic 180° hybrid blocks, good output isolation is expected for [17]. However, the isolation responses between

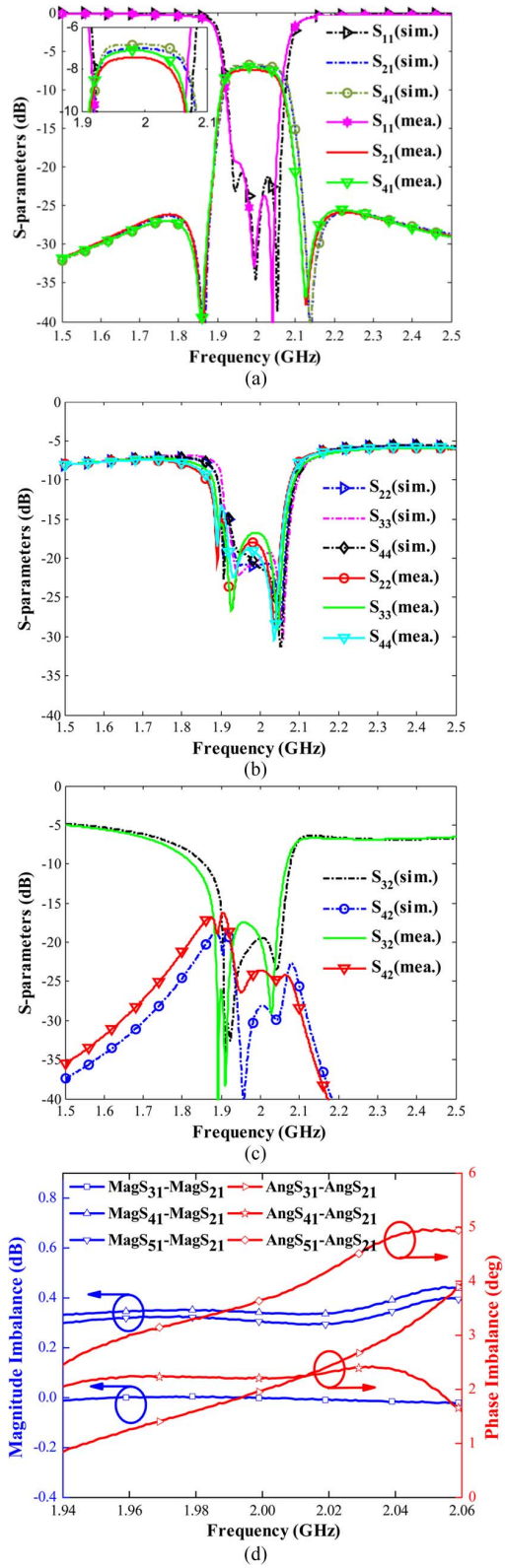

Fig. 14. Simulated and measured results (marked with "sim." and "mea.", respectively). (a) Insertion losses and the return loss of input port. (b) Return losses of output ports. (c) Isolations between output ports. (d) Measured magnitude and phase imbalances between output ports.

TABLE II
PERFORMANCE COMPARISON WITH PREVIOUS FOUR-WAY FILTERING POWER DIVIDERS

	Size ($\lambda_g \times \lambda_g$)	Filter order	Number of TZs	Central Frequency (GHz)	FBW (%)	Minimum IL (dB)	In-band RL (dB)	In-band output isolation (dB)
[12]	0.55×0.16	-	2	1.1	50	6+0.5	>10	>12
[13]-Fig. 10	~2.75×1.07	-	2	1.6 (first band)	11	6+0.8	>10	No consideration
[17]-Fig. 12	~6.37×3.13	5	0	11	3.6	~6+4	>17.5	No results
This work	**0.73×0.54**	**3**	**2**	**2**	**6**	**6+1.1**	**>16.7**	**>17.5**

the outputs of Ports 3 to 6 are not found in [17]. Our proposed filtering power divider is very suitable for four- and more- way applications in compact configurations, due to the inline and two-stage Wilkinson topology. With the frequency-dependent couplings and properly selected resistors, the performances of good frequency selectivity, matching and isolation are achieved simultaneously. The in-band RL and isolation are improved by 6.7 and 5.5 dB, respectively, when compared with [12]. Our measured in-band RL is a little lower than that in [17], while the occupied area of our filtering power divider is only about $1/50$ of the eight-port component in [17]. Thus, it can be regarded as a compromise between compactness and isolation performance.

IV. CONCLUSION

A four-way filtering power divider is proposed in this paper, which has a third-order generalized Chebyshev bandpass response. A filter is synthesized analytically in an inline topology with frequency-dependent couplings, realized by transmission-line resonators, open-ended stubs, and coupled lines. Then, the filter is extended to a four-way power divider with two power-dividing stages. Based on the even-/odd-mode analysis, the resistors are properly designed to achieve good matching and isolation between output ports. A microstrip prototype is developed, with reasonable agreement obtained between the simulated and measured results. Our proposed four-way filtering power divider has the advantages of low loss, high frequency selectivity, good in-band reflection and isolation. It is expected that the proposed design method and configuration can easily be extended to 2^{N-1}-way power dividers with N-th order filtering responses and more TZs.

REFERENCES

[1] S. Avrillon, I. Pele, A. Chousseaud, and S. Toutain, "Dual-band power divider based on semiloop stepped-impedance resonators," *IEEE Trans. Microw. Theory Techn.*, vol. 51, no. 4, pp. 1269–1273, Apr. 2003.

[2] J.-Y. Shao, S.-C. Huang, and Y.-H. Pang, "Wilkinson power divider incorporating quasi-elliptic filters for improved out-of-band rejection," *IET Electron. Lett.*, vol. 47, no. 23, pp. 1288–1289, Nov. 2011.

[3] X.-Y. Zhang, K.-X. Wang, and B.-J. Hu, "Compact filtering power divider with enhanced second-harmonic suppression," *IEEE Microw. Wireless Compon. Lett.*, vol. 23, no. 9, pp. 483–485, Sep. 2013.

[4] C.-F. Chen, T.-Y. Huang, T.-M. Shen, and R.-B. Wu, "Design of miniaturized filtering power dividers for system-in-a-package," *IEEE Trans. Compon. Packag. Manufact. Technol.*, vol. 3, no. 10, pp. 1663–1672, Oct. 2013.

[5] C.-F. Chen, C.-Y. Lin, B.-H. Tseng, and S.-F. Chang, "Microstrip bandpass power divider with high frequency selectivity and good in-band isolation," in *IEEE MTT-S Int. Microw. Symp. Dig.*, Tampa, FL, USA, Jun. 2014, pp. 1–3.

[6] P.-H. Deng and L.-C. Dai, "Unequal Wilkinson power dividers with favorable selectivity and high-isolation using coupled-line filter transformers," *IEEE Trans. Microw. Theory Techn.*, vol. 60, no. 6, pp. 1520–1529, Jun. 2012.

[7] Y.-C. Li, Q. Xue, and X.-Y. Zhang, "Single- and dual-band power dividers integrated with bandpass filters," *IEEE Trans. Microw. Theory Techn.*, vol. 61, no. 1, pp. 69–76, Jan. 2013.

[8] P.-H. Deng and Y.-T. Chen, "New Wilkinson power dividers and their integration applications to four-way and filtering dividers," *IEEE Trans. Microw. Theory Techn.*, vol. 4, no. 11, pp. 1828–1837, Nov. 2014.

[9] S.-W. Wong and L. Zhu, "Ultra-wideband power divider with good in-band splitting and isolation performances," *IEEE Microw. Wireless Compon. Lett.*, vol. 18, no. 8, pp. 518–520, Aug. 2008.

[10] K.-J. Song and Q. Xue, "Novel ultra-wideband (UWB) multilayer slotline power divider with bandpass response," *IEEE Microw. Wireless Compon. Lett.*, vol. 20, no. 1, pp. 13–15, Jan. 2010.

[11] S.-S. Gao, S. Sun, and S.-Q. Xiao, "A novel wideband bandpass power divider with harmonic-suppressed ring resonator," *IEEE Microw. Wireless Compon. Lett.*, vol. 23, no. 3, pp. 119–121, Mar. 2013.

[12] K.-J. Song, Y.-X. Mo, and Y. Fan, "Wideband four-way filtering-response power divider with improved output isolation based on coupled lines," *IEEE Microw. Wireless Compon. Lett.*, vol. 24, no. 10, pp. 674–676, Oct. 2014.

[13] R. Gomez-Garcia, M. Sanchez-Renedo, and J.-M. Munoz-Ferreras, "Microwave filtering power-distribution planar networks," in *IEEE MTT-S Int. Microw. Symp. Dig.*, Baltimore, MD, USA, Jun. 2011, pp. 1–4.

[14] L.-S. Wu, Y.-X. Guo, and J.-F. Mao, "Balanced-to-balanced Gysel power divider with band-pass filtering response," *IEEE Trans. Microw. Theory Techn.*, vol. 61, no. 12, pp. 40–52, Dec. 2013.

[15] C.-F. Chen and C.-Y. Lin, "Compact microstrip filtering power dividers with good in-band isolation performance," *IEEE Microw. Wireless Compon. Lett.*, vol. 24, no. 1, pp. 17–19, Nov. 2014.

[16] K.-X. Wang, X.-Y. Zhang, and B.-J. Hu, "Gysel power divider with arbitrary power ratios and filtering responses using coupling structure," *IEEE Trans. Microw. Theory Techn.*, vol. 62, no. 3, pp. 431–440, Mar. 2014.

[17] U. Rosenberg, M. Salehi, S. Amari, and J. Bornemann, "Compact multi-port power combination/distribution with inherent bandpass filter characteristics," *IEEE Trans. Microw. Theory Techn.*, vol. 62, no. 11, pp. 2659–2672, Nov. 2014.

[18] S. Amari and J. Bornemann, "Using frequency-dependent coupling to generate finite attenuation poles in direct-coupled resonator bandpass filters," *IEEE Microw. Guided Wave Lett.*, vol. 9, no. 10, pp. 404–406, Oct. 1999.

[19] Q.-X. Chu and H. Wang, "A compact open-loop filter mixed electric and magnetic coupling," *IEEE Trans. Microw. Theory Techn.*, vol. 56, no. 2, pp. 431–439, Feb. 2008.

[20] H. Wang and Q.-X. Chu, "An inline coaxial quasi-elliptic filter with controllable mixed electric and magnetic coupling," *IEEE Trans. Microw. Theory Techn.*, vol. 57, no. 3, pp. 667–673, Mar. 2009.

[21] W. Shen, L.-S. Wu, X.-W. Sun, W.-Y. Yin, and J.-F. Mao, "Novel substrate integrated waveguide filters with mixed cross coupling (MCC)," *IEEE Microw. Wireless Compon. Lett.*, vol. 19, no. 11, pp. 701–703, Nov. 2009.

[22] C.-L. Hsu and J.-T. Kuo, "Microstrip realization of trisection synthesis with frequency-dependent admittance inverter," *Progr. Electromagn. Res*, vol. 113, pp. 195–210, 2011.

[23] L. Szydlowski, A. Lamecki, and M. Mrozowski, "Coupled-resonator filters with frequency-dependent couplings: coupling matrix synthesis," *IEEE Microw. Wireless Compon. Lett.*, vol. 22, no. 6, pp. 312–314, Jun. 2012.

[24] N. Leszczynska, L. Szydlowski, and M. Mrozowski, "A novel synthesis technique for microwave bandpass filters with frequency-dependent couplings," *Progr. Electromagn. Res.*, vol. 137, pp. 35–50, 2013.
[25] L. Szydlowski, N. Leszczynska, and M. Mrozowski, "Generalized Chebyshev bandpass filters with frequency-dependent couplings based on stubs," *IEEE Trans. Microw. Theory Techn.*, vol. 61, no. 10, pp. 3601–3612, Oct. 2013.
[26] L. Szydlowski, A. Lamecki, and M. Mrozowski, "A novel coupling matrix synthesis technique for generalized Chebyshev filters with resonant source-load connection," *IEEE Trans. Microw. Theory Techn.*, vol. 61, no. 10, pp. 3568–3577, Oct. 2013.
[27] M. Salehi, J. Bornemann, and E. Mehrshahi, "Substrate integrated waveguide band pass filters with frequency-dependent coupling elements," *Int. J. RF Microw. Comput.-Aided Eng.*, vol. 24, no. 2, pp. 237–242, Mar. 2014.
[28] X.-L. Wang, I. Sakagami, and M. Yoshikawa, "Planar dual-band fork three-way power dividers with inductor-terminated transmission lines," in *Proc. Asia–Pacific Microw. Conf.*, Sendai, Japan, Nov. 2014, pp. 825–827.
[29] J. Zhou, K. A. Morris, and M. J. Lancaster, "General design of multi-way multi-section power dividers by interconnecting two-way dividers," *IEEE Trans. Microw. Theory Techn.*, vol. 55, no. 10, pp. 2208–2215, Oct. 2007.
[30] Y. Xu and R. G. Bosisio, "Design of multiway power divider by using stepped-impedance transformers," *IEEE Trans. Microw. Theory Techn.*, vol. 60, no. 9, pp. 2781–2790, Sep. 2012.

Feng-Jun Chen was born in Chongqing, China, in 1989. He received the B.S. degree in tourism management from Southeast University, Nanjing, China, in 2012, and the M.S. degree in electromagnetic fields and microwave technologies from Shanghai Jiao Tong University, Shanghai, China, in 2015.

He is currently an Engineer with the Microsystem and Terahertz Research Center, China Academy of Engineering Physics, Chengdu, China. His research interest includes the design and synthesis of miniaturized microwave filters, and terahertz technology.

Lin-Sheng Wu (S'09–M'10–SM'15) was born in 1981. He received the B.S. degree in electronic and information engineering and M.S. and Ph.D. degrees in electromagnetic fields and microwave technologies from Shanghai Jiao Tong University, Shanghai, China, in 2003, 2006, and 2010, respectively.

From February 2010 to January 2012, he was a Post-Doctoral Fellow with Shanghai Jiao Tong University (SJTU), Shanghai, China. From August to November 2010 and from December 2012 to December 2013, he was a Research Fellow with the Department of Electrical and Computer Engineering, National University of Singapore, Singapore. He is currently an Associate Professor with the Key Laboratory of Ministry of Education of Design and Electromagnetic Compatibility of High Speed Electronic Systems, SJTU, where his present research interest is mainly focused on novel techniques for microwave integration, passive components and carbon nano-electromagnetics. He has authored or coauthored approximately 100 technical papers.

Dr. Wu is a reviewer of several international journals, including five IEEE Transactions and Letters.

Liang-Feng Qiu was born in Hangzhou, China, in 1985. He received the B.S. degree in optical information science and technology and M.S. degree in circuits and systems from Hangzhou Dianzi University, Hangzhou, in 2008 amd 2010, respectively. He is currently working toward the Ph.D. degree in electromagnetic fields and microwave technologies at the Key Laboratory of Ministry of Education of Design and EMC of High-Speed Electronic Systems, Shanghai Jiao Tong University, Shanghai, China.

His current research is focused on the passive components, especially the synthesis and design of microwave filters.

Jun-Fa Mao (M'92–SM'98–F'12) was born in 1965. He received the B.S. degree in radiation physics from the University of Science and Technology of National Defense, Changsha, China, in 1985, the M.S. degree in experimental nuclear physics form Shanghai Institute of Nuclear Research, Shanghai, China, in 1988, and the Ph.D. degree in electronic engineering from Shanghai Jiao Tong University, Shanghai, in 1992.

Since 1992, he has been a Faculty Member in Shanghai Jiao Tong University, Shanghai, China, where he is currently a Chair Professor and the Executive Dean of the School of Electronic, Information and Electrical Engineering. He was a Visiting Scholar with the Chinese University of Hong Kong, Hong Kong, from 1994 to 1995, and a Postdoctoral Researcher with the University of California, Berkeley, CA, USA, from 1995 to 1996. He has authored or coauthored more than 200 journal papers (including 80 IEEE journal papers) and 120 international conference papers. His research interests include the interconnect and package problem of integrated circuits and systems, analysis and design of microwave circuits.

Dr. Mao was the recipient of the National Natural Science Award of China in 2004, the National Technology Invention Award of China in 2008, the National Science and Technology Progress Award of China in 2012, and the Best Paper Award of 2008 Symposium of APEMC in conjunction with 19th International Symposium of Zurich EMC. He is a Chief Scientist with the National Basic Research Program (973 Program) of China, a project leader of the National Science Foundation for Creative Research Groups of China, a Cheung Kong Scholar of the Ministry of Education, China, an Associate Director of the Microwave Society of China Institute of Electronics, the 2007–2009 Chair of the IEEE Shanghai Section, and the 2009–2011 Chair of IEEE MTT Shanghai Chapter.